Chin. Geogra. Sci. 2022 Vol. 32 No. 5 pp. 759−775
https://doi.org/10.1007/s11769-022-1299-8

Springer Science Press
www.springerlink.com/content/1002-0063

Remote Sensing-based Spatiotemporal Distribution of Grassland Aboveground Biomass and Its Response to Climate Change in the Hindu Kush Himalayan Region

XU Cong[1, 2], LIU Wenjun[3], ZHAO Dan[1, 2], HAO Yanbin[4, 5, 6], XIA Anquan[7], YAN Nana[1], ZENG Yuan[1, 2]

(1. *State Key Laboratory of Remote Sensing Science*, *Aerospace Information Research Institute*, *Chinese Academy of Sciences*, *Beijing* 100101, *China*; 2. *University of Chinese Academy of Sciences*, *Beijing* 100049, *China*; 3. *School of Ecology and Environmental Sciences & Yunnan Key Laboratory for Plateau Mountain Ecology and Restoration of Degraded Environments*, *Yunnan University*, *Kunming* 650091, *China*; 4. *College of Life Sciences*, *University of Chinese Academy of Sciences*, *Beijing* 100049, *China*; 5. *CAS Center for Excellence in Tibetan Plateau Earth Sciences*, *Chinese Academy of Sciences*, *Beijing* 100101, *China*; 6. *Beijing Yanshan Earth Critical Zone National Research Station*, *University of Chinese Academy of Sciences*, *Beijing* 101408, *China*; 7. *College of Resources and Environment*, *University of Chinese Academy of Sciences*, *Beijing* 100049, *China*)

Abstract: The grassland in the Hindu Kush Himalayan (HKH) region is one of the largest and most biodiverse mountain grassland types in the world, and its ecosystem service functions have profound impacts on the sustainable development of the HKH region. Monitoring the spatiotemporal distribution of grassland aboveground biomass (AGB) accurately and quantifying its response to climate change are indispensable sources of information for sustainably managing grassland ecosystems in the HKH region. In this study, a pure vegetation index model (PVIM) was applied to estimate the long-term dynamics of grassland AGB in the HKH region during 2000–2018. We further quantified the response of grassland AGB to climate change (temperature and precipitation) by partial correlation and variance partitioning analyses and then compared their differences with elevation. Our results demonstrated that the grassland AGB predicted by the PVIM had a good linear relationship with the ground sampling data. The grassland AGB distribution pattern showed a decreasing trend from east to west across the HKH region except in the southern Himalayas. From 2000 to 2018, the mean AGB of the HKH region increased at a rate of 1.57 g/(m^2·yr) and ranged from 252.9 (2000) to 307.8 g/m^2 (2018). AGB had a positive correlation with precipitation in more than 80% of the grassland, and temperature was positively correlated with AGB in approximately half of the region. The change in grassland AGB was more responsive to the cumulative effect of annual precipitation, while it was more sensitive to the change in temperature in the growing season; in addition, the influence of climate varied at different elevations. Moreover, compared with that of temperature, the contribution of precipitation to grassland AGB change was greater in approximately 60% of the grassland, but the differences in the contribution for each climate factor were small between the two temporal scales at elevations over 2000 m. An accurate assessment of the temporal and spatial distributions of grassland AGB and the quantification of its response to climate change are of great significance for grassland management and sustainable development in the HKH region.

Keywords: grassland aboveground biomass (AGB); climate change; elevation; spatiotemporal distribution; Hindu Kush Himalayan (HKH) region

Citation: XU Cong, LIU Wenjun, ZHAO Dan, HAO Yanbin, XIA Anquan, YAN Nana, ZENG Yuan, 2022. Remote Sensing-based Spatiotemporal Distribution of Grassland Aboveground Biomass and Its Response to Climate Change in the Hindu Kush Himalayan Region. *Chinese Geographical Science*, 32(5): 759−775. https://doi.org/10.1007/s11769-022-1299-8

Received date: 2022-05-03; accepted date: 2022-08-10

Foundation item: Under the auspices of the Strategic Priority Research Program of the Chinese Academy of Sciences (No. XDA19030202), National Key Research and Development Program of China (No. 2020YFE0200800), International Cooperation and Exchange of National Natural Science Foundation of China (No. 31761143018), National Natural Science Foundation of China (No. 42071344)

Corresponding author: ZHAO Dan. E-mail: zhaodan@aircas.ac.cn

1 Introduction

The Hindu Kush Himalayan (HKH) region is a unique mountain ecosystem and is regarded as a pivotal region in terms of ecosystem services, biodiversity, carbon and water cycles and climate change (Chen et al., 2013; Shrestha et al., 2016; Kandel et al., 2021). As the largest ecosystem type in the HKH region, grassland plays an important role in the ecosystem services and sustainability of the area (Xu et al., 2009; 2019). However, the grassland ecosystem in the region is experiencing impacts from global climate change, land cover change and population growth (Wester et al., 2019). For example, the grassland has been degraded to varying degrees due to physical and anthropogenic factors in recent decades (Xu et al., 2008; Ran et al., 2019). Consequently, the function of the grassland ecosystem in the HKH region has been severely affected, endangering the sustainable development of the region (Wick et al., 2016; Dimri et al., 2020). As two of the most direct indicators of grassland ecosystem functioning, the temporal dynamics and spatial distribution of grassland aboveground biomass (AGB) in the HKH region and their response to climate change must be assessed so that the regional carbon cycle can be determined and the sustainable utilization of grassland resources can occur.

Remote sensing has been widely applied to grassland AGB estimation due to it having a higher efficiency level and better spatiotemporal data continuity than the field survey methods at a large scale (Todd et al., 1998; Psomas et al., 2011; Jin et al., 2014; Yang et al., 2018). Grassland AGB estimation models or methods based on remote sensing can be divided into three categories: statistical models based on vegetation indices (Guerini et al., 2019; Yu et al., 2021), an assimilation of model and data approaches (Quan et al., 2017) and machine learning models (Morais et al., 2021; Zeng et al., 2021). By comparison, establishing relationships between different vegetation indices (VIs) and AGB measured in field plots is the most common and simple approach for grassland AGB estimation over a large area. For example, Ge et al. (2018) indicated that the normalized difference vegetation index (NDVI) and enhanced vegetation index (EVI) of Moderate Resolution Imaging Spectroradiometer (MODIS) predicted grassland AGB well in the source region of the Yellow River. The NDVI also performed well in the hinterland and mountainous areas of the Tibetan Plateau (Kong et al., 2019; Wei et al., 2021). However, the estimation of grassland AGB based on VIs might be influenced by the spectral saturation in dense vegetation areas and mixed background information, such as soil (Li et al., 2016). Some models or indices have been proposed to estimate grassland AGB more accurately by reducing the influence of soil and other background factors (Xu et al., 2021). For example, the pure vegetation index model (PVIM) extracted vegetation information by spectral mixed analysis (SMA) based on multitemporal remote sensing data and this approach was proven to be more advantageous in estimating grassland AGB with varied fractional coverage (Li et al., 2016). Nevertheless, limited by sampling data and remote sensing data, most of the current studies on the remote sensing estimation of grassland AGB in the HKH region were focused on the Qinghai-Tibet Plateau (Jiao et al., 2017; Liu et al., 2017a; Tang et al., 2021) and the spatial and temporal distribution and dynamic changes in grassland AGB in the HKH region were unclear.

Grassland AGB is easily influenced by climate factors, which has been confirmed by many previous studies (Sun et al., 2013; Li et al., 2018; Zhou et al., 2021). As one of the most unique regions in the world, climate change in the HKH region is evident, and an example was the general increase in extreme warm events over the entire HKH region during 1961–2015 (Sun et al., 2017), which severely affected the growth of the grassland in this region (Panday and Ghimire 2012; Wester et al., 2019). Several studies have revealed the response of grassland AGB to climate change in this region. For example, Dai et al. (2019) demonstrated that the AGB of alpine meadow was dominated by mean annual precipitation (MAP) during 2008–2017 at the Haibei National Field Research Station on the northeastern Tibetan Plateau of China. Wang et al. (2018) showed that the response of grassland AGB to temperature and precipitation changes in different months was not consistent in Qinghai Province of China during 2003–2016. However, these studies focused more on local areas or some specific areas rather than on the whole region; thus, there is still a lack of systematic research on the response of grassland AGB to climate change in the whole region. Moreover, the difference in the effect of climatic conditions on grassland AGB at the annual scale or in different periods is also unclear in

this region. In addition, the terrain has an impact on grassland AGB as it influences hydrothermal conditions (Duparc et al., 2013; Carlyle et al., 2014). Besides, the complex topographic conditions in the HKH region cause inconsistent response of grassland AGB to climate change in different regions, especially at different elevation gradients (Duparc et al., 2013; Karimi et al., 2021). Thus, a quantification of the effect of elevation on grassland AGB response to climate change is needed at a large scale.

Therefore, the main purpose of this paper is to evaluate the spatial and temporal distributions of grassland AGB in the HKH region and quantify the response of grassland AGB to climate change. To achieve this goal, we: 1) assessed the applicability of the PVIM for estimating grassland AGB in the HKH region and verified its accuracy based on the ground-measured data; 2) estimated the spatial distribution of grassland AGB in the HKH region from 2000 to 2018 with the PVIM based on long time series MODIS data and analyzed its interannual variation through trend analysis; and 3) quantified the effects of precipitation and temperature on the variation in grassland AGB through variance partitioning analysis (VPA) and partial correlation analysis and further compared the difference in this effect at different elevation ranges. This study of spatial and temporal variation of grassland AGB and its response to climate change can provide theoretical basis for strategies adjusting and management optimizing of grassland ecosystem in HKH region.

2 Materials and Methods

2.1 Study area

The HKH region is in the southern of Asia (16°N–40°N, 61°E–105°E) and spans over 4 million km^2, including all Bhutan and Nepal and parts of Afghanistan, Bangladesh, China, India, Myanmar and Pakistan (Fig. 1). The HKH region has the highest and largest mountain system in the world with an elevation range from sea level to over 8000 m, which is referred to as the 'Third Pole', and thus creates one of the most diverse ecosystems in the world providing various ecosystem products and services (Singh et al., 2011; Yao et al., 2012; Xu et al., 2019). Grassland is one of the largest ecosystem types in the region, accounting for over 60% of the total area according to previous studies (Dong et al., 2010; Xu et al., 2019). The grassland in HKH region is mainly distributed on the Qinghai-Tibet Plateau, the Hindu Kush Mountains and the southern Himalayas (Fig. 1). The climate is mainly dominated by both the monsoon of South Asia and midlatitude westerlies (Schickhoff et al., 2015). In particular, the precipitation is uneven with a great spatial difference between the south and north, which is caused by the complex terrain. The average annual temperature in the region also varies greatly in its spatial distribution and even from place to place due to the rapid changes in elevation. At the same time, as a

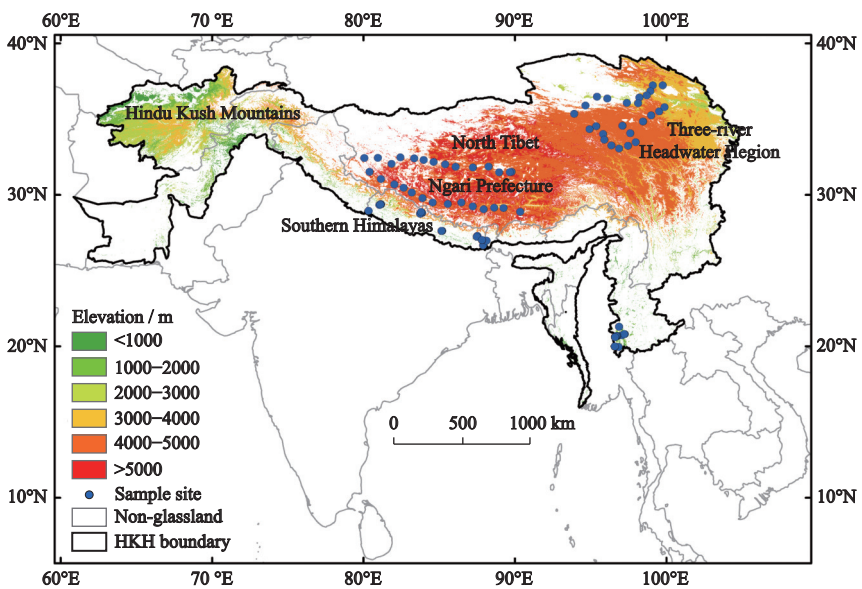

Fig. 1 Location of the Hindu Kush Himalayan (HKH), sample sites and the distribution of the grassland by elevation

vulnerable area to climate change, the HKH region has shown a significant warming trend with 0.176°C per decade in the past 100 yr (Ren et al., 2017).

2.2 Data source

2.2.1 Remote sensing data

The MODIS 8-day data sets (MOD09Q1) with a 250 m spatial resolution during the growing season (from early April to late September) of each year from 2000 to 2018, covering the whole HKH region, were obtained and preprocessed in the Google Earth Engine (GEE) platform (Table 1). MODIS land cover type products (MCD12Q1) with a 500 m spatial resolution were used in our study to extract the spatial distribution of the grassland in the HKH region, and the global vegetation classification scheme of the International Geosphere-Biosphere Programme (IGBP) was adopted for selecting the grassland, which showed an accuracy of over 70% based on an evaluation by a previous study (Yang et al., 2017). The preprocessing involved data splicing and clipping and was completed on the GEE platform. In addition, we constructed a simple decision mechanism in which only the pixels whose land cover type was grassland for more than ten years during the monitoring period were used in the subsequent analysis. Then, we used a simple overlay analysis by IDL 8.5 to extract the 250 m MODIS data for the grassland region in the HKH region based on the grassland mask.

The digital elevation model (DEM) was obtained from the Shuttle Radar Topography Mission (SRTM) with an absolute accuracy of better than 16 m within a 90 m spatial resolution (Jarvis et al., 2008). The SRTM data performed well, with an absolute height error of 6.2 m in Asia (Rodríguez et al., 2006). The elevation was then extracted from the DEM. To match the MODIS data, the elevation data were resampled to 250 m.

2.2.2 Meteorological datasets

The monthly meteorological data (precipitation and temperature) with a 0.04° spatial resolution were obtained from WorldClim (https://www.worldclim.org), which is a database of high spatial resolution global climate data (Table 1) (Fick and Hijmans, 2017). The monthly precipitation and maximum and minimum temperature data were used to calculate the accumulated precipitation and mean temperature for each year from 2000–2018, respectively. Additionally, we calculated the accumulated precipitation and mean temperature of the growing season for each year.

2.2.3 Field data

Field data surveys were conducted in 2015 and 2018, in Qinghai-Tibet Plateau of China, Nepal and Myanmar (Fig. 1). At each site, five sample plots (1 m × 1 m) distributed regularly within 100 m^2 were collected. Grassland AGB was acquired by harvesting all aboveground portions of vegetation within the sample plot. In addition, the geographic coordinates were accurately recorded by a Trimble GeoXH 3000 handheld GPS with centimeter-level position accuracy. The mean value of grassland AGB at each site was used for modeling and validation. However, there were some sites where it was difficult to collect in five plots, so we only calculated the mean value of AGB for the plots where data were collected. A total of 112 sites with 461 sample plots were collected.

2.3 Methods

2.3.1 Pure vegetation index model

The theoretical basis of the PVIM is to enhance the vegetation signal while reducing the background information of soil by spectral mixture analysis (SMA). According to the SMA, the pixel information was decomposed:

$$VR = MR - (1 - FVC) \times SR \quad (1)$$

where VR and SR represent the reflected signals of vegetation and soil, respectively. MR is the reflected signal of the whole pixel, which is generally regarded as

Table 1 Description of remote sensing data and meteorological data for the Hindu Kush Himalayan (HKH) region

Data	Spatial resolution	Temporal resolution	Time span	Data source
MOD09Q1	250 m	8-d	2000–2018	NASA LPDAAC at the USGS EROS Center (https://lpdaac.usgs.gov/data/)
Landcover (MCD12Q1)	500 m	Yearly	2000–2018	NASA LPDAAC at the USGS EROS Center (https://lpdaac.usgs.gov/data/)
Elevation	90 m	–	2000	NASA/CGIAR (https://srtm.csi.cgiar.org/)
Temperature	0.04°	Monthly	2000–2018	WorldClim (https://www.worldclim.org)
Precipitation	0.04°	Monthly	2000–2018	WorldClim (https://www.worldclim.org)

mixed information; *FVC* represents fractional vegetation coverage and it is calculated by a pixel dichotomy model (Adams et al., 1986).

It is generally believed that the vegetation index (VI) reduces the influence of atmospheric and soil information on vegetation to a certain degree (Li et al., 2016). Therefore, VI could be used to replace the reflected signals in Eq. (1) and ratio vegetation index (*RVI*) performed better for the grassland AGB estimation (Eq. (2) and Eq. (3)), which was verified in a previous study (Li et al., 2016).

$$RVI = \frac{NIR}{R} \tag{2}$$

$$PRVI = RVI_{vs} - (1 - FVC) \times RVI_{soil} \tag{3}$$

where near-infrared (*NIR*) and red (*R*) are the reflectance of the near-infrared band and red band, respectively. *PRVI* is the pure vegetation index of each pixel; RVI_{vs} is the *RVI* value of the vegetation-soil mixed pixel and RVI_{soil} is the value of each pixel at the beginning of the growth season, which is early April in our study.

After filtering the background signal or non-vegetation signal, the common simple linear model was used to estimate the AGB of the grassland as followed:

$$AGB = a \times PRVI + b \tag{4}$$

where *a* and *b* are the parameters of the common linear model calculated based on sample data.

Because the *PRVI* was the result of soil filtering, a simpler functional form was expressed as:

$$AGB = M \times PRVI \tag{5}$$

where *M* is a single conversion factor relating the *PRVI* to *AGB*, which was measured in g/m^2.

The coefficient of determination (R^2) and root mean squared error (*RMSE*) were used to evaluate the performance of the *PVIM* and were calculated as:

$$R^2 = \frac{\sum (\hat{y}_i - \bar{y})^2}{\sum (y_i - \bar{y})^2} \tag{6}$$

$$RMSE = \sqrt{\frac{\sum_{i=1}^{n} (\hat{y}_i - y_i)^2}{n}} \tag{7}$$

where $\hat{y}_i$ and y_i are the predicted values of the AGB and measured values of AGB, respectively; $\bar{y}$ is the mean value of measured AGB and *n* is the number of sample plots.

2.3.2 *Trend analysis of grassland aboveground biomass*

Trend analysis is a method used to predict the change in grassland AGB by linear regression analysis over the monitoring period and the change was calculated as follows:

$$Slope = \frac{n \times \sum_{i=1}^{n} i \times AGB_i - \left(\sum_{i=1}^{n} i\right)\left(\sum_{i=1}^{n} AGB_i\right)}{n \times \sum_{i=1}^{n} i^2 - \left(\sum_{i=1}^{n} i\right)^2} \tag{8}$$

where *Slope* is the slope of the regression equation of each pixel and *i* represents 1, 2, 3, …, *n*, for the year from 2000 to 2018 and *n* is the time span, which is 19 in our study. AGB_i is the mean value of AGB in year *i*. When *Slope* is greater than 0, it indicates that the grassland AGB of this pixel is increasing. When *Slope* is equal to 0, it indicates that the AGB is basically unchanged; When *Slope* is less than 0, it indicates that the grassland AGB of the pixel is decreasing.

To detect the significance of the change trend in grassland AGB, a nonparametric Mann-Kendall (M-K) method was applied. The M-K method did not assume that the samples followed a certain distribution and was not affected by a few outliers, and it is more suitable for time-series variables. The calculation process of the M-K method can be described as follows:

$$\operatorname{sgn}(q_j - q_i) = \begin{cases} 1, \text{ if } q_j - q_i > 0 \\ 0, \text{ if } q_j - q_i = 0 \\ -1, \text{ if } q_j - q_i < 0 \end{cases} \tag{9}$$

$$S = \sum_{i=1}^{n-1} \sum_{j=i+1}^{n} \operatorname{sgn}(q_j - q_i) \tag{10}$$

$$\operatorname{var}(S) = \frac{n(n-1)(2n+5) - \sum_{i=1}^{m} t_i(t_i - 1)(2t_i + 5)}{18} \tag{11}$$

$$Z = \begin{cases} \dfrac{S-1}{\sqrt{\operatorname{var}(S)}} & \text{if } S > 0 \\ 0 \text{ if } S = 0 \\ \dfrac{S+1}{\sqrt{\operatorname{var}(S)}} & \text{if } S < 0 \end{cases} \tag{12}$$

where q_i and q_j are the grassland AGB in years *i* and *j* ($j > i$), respectively. sgn is a symbolic function. *n* is the time span. t_i represents the number of tied groups in ex-

tent i and a tied group represents a sample data set with the same AGB value. S is a statistic that follows a normal distribution and var(S) is variance. Z represents the statistic of the M-K test. If $|Z| \geq Z_{1-\alpha/2}$ for a given significance level α ($\alpha = 0.05$ in our study), then the grassland AGB time-series data would show a significant increasing or decreasing trend.

2.3.3 *Partial correlation analysis*

Partial correlation analysis is usually used to analyze the linear correlation between two variables while controlling for the linear influence of other variables. This method could be used to analyze the response of vegetation to a single climatic factor, and we used the partial correlation coefficient to measure the degree of correlation between two variables, which can be calculated as follows:

$$r_{xy(z)} = \frac{r_{xy} - r_{xz}r_{yz}}{\sqrt{1-r_{xz}^2}\sqrt{1-r_{yz}^2}} \tag{13}$$

where $r_{xy(z)}$ is the partial correlation coefficient of variable x and variable y after excluding the influence of variable z. r_{xy}, r_{yz} and r_{xz} represent the simple correlation coefficients between pairs of three variables (AGB, temperature and precipitation, respectively). The simple correlation coefficient is generally the Pearson correlation coefficient, which can be calculated by:

$$r_{xy} = \frac{\sum_{i=1}^{n}(x_i-\bar{x})(y_i-\bar{y})}{\sqrt{\sum_{i=1}^{n}(x_i-\bar{x})^2}\sqrt{\sum_{i=1}^{n}(y_i-\bar{y})^2}} \tag{14}$$

where x and y are the pairs of three variables; x_i and y_i are the values of variables x and y in year i, respectively; and $\bar{x}$ and $\bar{y}$ represent the mean values of variables x and y from 2000 to 2018.

A bilateral t test (Eq. (15)) was applied to infer the significance of the partial correlation coefficient at a significance level of 0.05.

$$t = \frac{r\sqrt{m-k-2}}{\sqrt{1-r^2}} \tag{15}$$

where r is the partial correlation coefficient, and k is the number of controllable variables.

2.3.4 *Variance partitioning analysis*

VPA is a contribution decomposition method based on the regression equation, which can calculate the contribution of each variable for a regression equation with J independent variables. After estimating the combined effects of temperature and precipitation on the interannual variation in grassland AGB based on multiple linear regression, we used VPA to quantitatively analyze the respective contributions of the two climate factors. The contribution decomposition formulas are listed as follows:

$$y = a + \sum_{j=1}^{J} b_j x_j + e \tag{16}$$

$$1 = \sum_{j=1}^{J} b_j \frac{\mathrm{cov}(x_i, y)}{\mathrm{var}(y)} + \frac{\mathrm{cov}(e, y)}{\mathrm{var}(y)} \tag{17}$$

where x_j and b_j are the independent variable j and its coefficient of linear regression, respectively; $b_j \frac{\mathrm{cov}(x_i, y)}{\mathrm{var}(y)}$ is the contribution of the independent variable j to the variation in y; and $\sum_{j=1}^{J} b_j \frac{\mathrm{cov}(x_i, y)}{\mathrm{var}(y)}$ is the fit of the regression equation. cov(x_i, y) and var(y) are the covariance and variance, respectively.

3 Results

3.1 Performance of the PVIM

Both the linear relationship and proportional relationship between the grassland AGB and PRVI were established in our study (Fig. 2a). The result showed that the linear relationship (R^2 = 0.81, *RMSE* = 109.8, n = 78) performed better than the proportional relationship (R^2 = 0.79, *RMSE* = 117.4, n = 78). Then, we evaluated the accuracy of the linear relationship for the grassland AGB estimation in the whole HKH region by comparing the predicted AGB with the measurements of the ground sample plots shown in Fig. 2b. Our results indicated a reliable performance of the PVIM in estimating grassland AGB, with R^2 values of 0.60 ($P < 0.01$, n = 66) and 0.51 ($P < 0.01$, n = 46) verified by ground sample points collected in 2015 and 2018, respectively.

3.2 Spatial distribution of grassland AGB and its change along elevation

There was obvious spatial heterogeneity in the mean annual grassland AGB in the HKH region from 2000 to 2018 (Fig. 3). Overall, grassland AGB showed a decreasing trend from east to the west throughout this re-

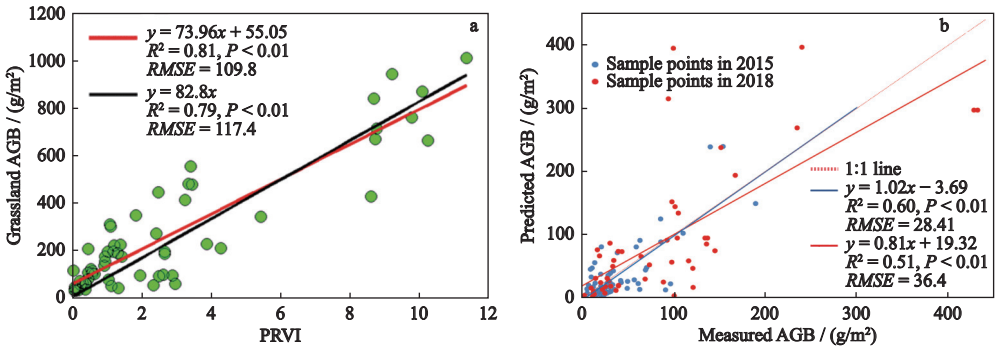

Fig. 2 Relationships between the pure ratio vegetation index (PRVI) and grassland aboveground biomass (AGB) (a), the red and black lines represent the different linear simulation curves, respectively; and the validation of the grassland AGB predicted by the pure vegetation index model (b)

gion, except in the southern Himalayas, where AGB was relatively high. According to our statistical results, the mean annual grassland AGB in the whole HKH region was 274.7 g/m^2 during 2000–2018. At the subregional scale, both the eastern part of the Qinghai-Tibet Plateau and the southern side of the Himalayas showed high grassland AGB values of over 400 g/m^2, covering approximately 20.4% of the area. Low grassland AGB values (< 50 g/m^2) were mainly distributed in the central part of the Qinghai-Tibet Plateau and the western part of the HKH region, accounting for approximately 25.8% of the grassland area.

Furthermore, we also analyzed the variation in grassland AGB along altitudinal gradients (Fig. 4). The mean annual grassland AGB showed a decreasing tendency in the ranges of 0 to 3000 m and 3000 m to 7000 m. Among the six elevation ranges, the mean grassland AGB was the highest (362.9 g/m^2) in the range of 3000 to 4000 m, while the lowest appeared at elevations above 5000 m (101.3 g/m^2). The total grassland AGB (159.9 Tg) presented an approximate parabolic trend with the change in elevation range due to the discrepancy in grassland area occupied between the different elevation ranges. The grassland at the elevation range of 4000–5000 m contributed the most to the regional total AGB (84.9 Tg, 53.1%), followed by that in the range of 3000–4000 m at 31.3%. Because of the small grassland area (< 3000 m) or low mean AGB (> 5000 m) in the remaining elevation ranges, these areas accounted for only 15.6% of the total grassland AGB.

Additionally, the mean annual grassland AGB within the same elevation range showed differences in terms of the standard deviation coefficient (Fig. 4). The largest variation in grassland AGB occurred in the elevation range of 4000–5000 m, at 111%, followed by that in the range above 5000 m and 3000–4000 m, at 106% and 98%, respectively. There were similar differences among the remaining three elevation ranges, with standard deviation coefficients from 62% to 70%.

3.3 Interannual variation of grassland AGB and its difference between different elevation ranges

The trend of the annual regional grassland AGB from 2000 to 2018 was shown in Fig. 5, and there was a sig-

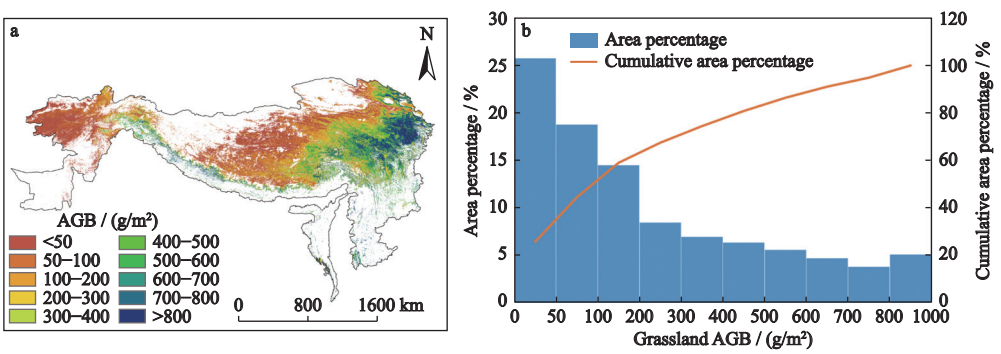

Fig. 3 Spatial distribution of the mean annual grassland aboveground biomass (AGB) from 2000 to 2018 in the Hindu Kush Himalayan (HKH) region (a) and the area percentage and cumulative area percentage of grassland AGB (b)

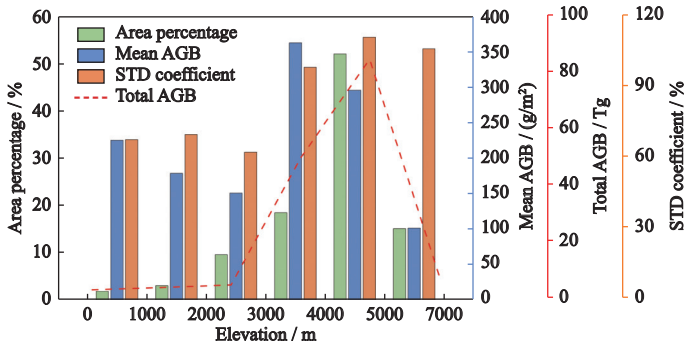

Fig. 4 Grassland area percentage, mean aboveground biomass (AGB), total AGB and standard deviation coefficient of AGB at different elevation ranges from 2000 to 2018 in the HKH region

nificant increasing trend with a rate of 1.57 g/(m^2·yr) (R^2 = 0.33). Between 2000 and 2018, the maximum mean AGB in the region was 307.8 g/m^2 (2018), while the minimum mean AGB was 252.9 g/m^2 (2000). Then, we obtained the trend of the annual AGB during 2000–2018 across the HKH region by applying slope trend analysis and the M-K significance test at the level of 0.05 (Fig. 6). Our results showed that grassland AGB in most areas of HKH had an increasing or significant increasing trend, which accounted for approximately 52.8% and 13.2% of the grassland area of the HKH region, respectively. The mean rate of the grassland AGB with a significant increasing trend was 5.9 g/m^2 per year, and the increasing trends were mainly distributed in the northeastern part of the Qinghai-Tibet Plateau. The grassland area with a decreasing trend accounted for 29.6% of the HKH grassland area and was mainly located in the central part of the Qinghai-Tibet Plateau, while only 4.4% of grassland experienced significantly reduced AGB.

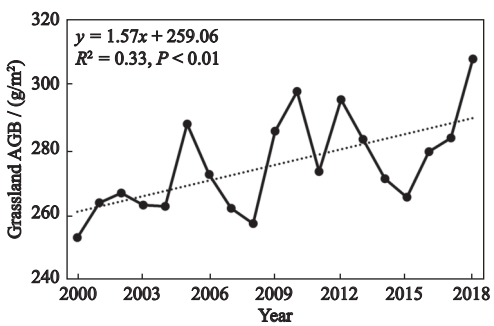

Fig. 5 Interannual variation of the mean grassland aboveground biomass (AGB) in the HKH region from 2000 to 2018

The area percentages of the four grassland AGB change trends varied at different elevation ranges (Fig. 7). Among the elevation range of 1000 to 4000 m, the AGB of over 80% grassland areas showed increasing or significant increasing trends. By comparison, the grassland areas with an increasing or significant increasing trend of AGB accounted for only 47.3% and 51.7% of the elevation ranges below 1000 m and over 5000 m, respectively, which were approximately equal to that with a decreasing or significant decreasing trend (52.7% and 48.3%). Moreover, the grassland AGB showed a decreasing or significant decreasing trend in approxim-

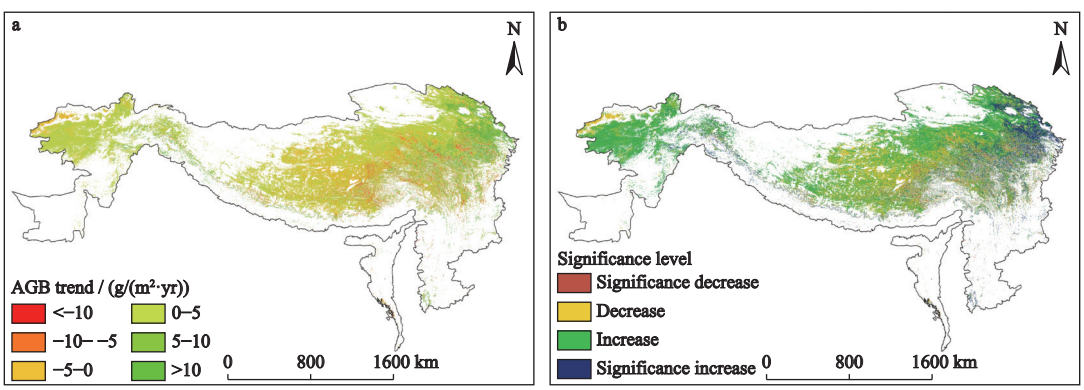

Fig. 6 Aboveground biomass (AGB) trend in the HKH region from 2000 to 2018 (a) and the significance level of the grassland AGB interannual trend (P < 0.05) (b)

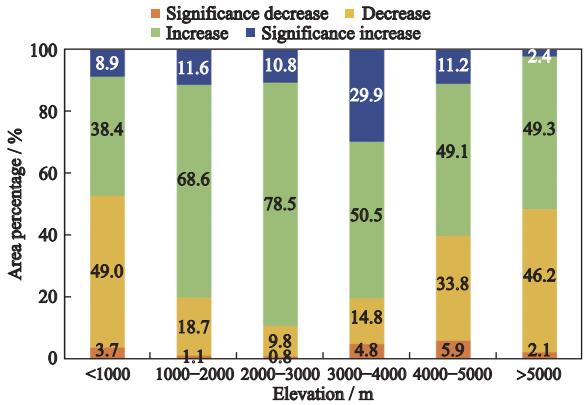

Fig. 7 Area percentage of the four interannual variation trends of grassland aboveground biomass at different elevation ranges from 2000 to 2018

ately 40% of grassland in the elevation range of 4000–5000 m. However, the decreasing trend of grassland AGB was significant in only a few areas at all elevation ranges.

3.4 Response of grassland AGB to climate change

To explore the differences in the spatial distribution of grassland AGB in response to climate change, we calculated the partial correlation at the significance level of 0.05 between them at the two temporal scales separately. The spatial distribution of the response of grassland AGB to each climate factor in the HKH region showed some similarity between the two temporal scales (Fig. 8). Precipitation was positively correlated with AGB at both temporal scales over 80% of the grassland in the HKH region. In contrast, temperature was negatively correlated with AGB on the central Tibetan Plateau and in the western HKH region, and these areas occupied approximately half of the grassland. Additionally, there was no significant spatial difference for the effect of climate factors on grassland AGB variation between the two temporal scales.

Further analysis showed that the partial correlations between the climate factors and grassland AGB varied with elevation (Fig. 9). In terms of the annual scale, the mean annual precipitation had a significant positive correlation with AGB over 70% of the grassland areas at elevations below 1000 m, and the area percentage decreased with elevation (Fig. 9a). By comparison, the area percentage of grassland with a significant positive correlation between temperature and AGB showed a parabolic trend with elevation and reached its highest

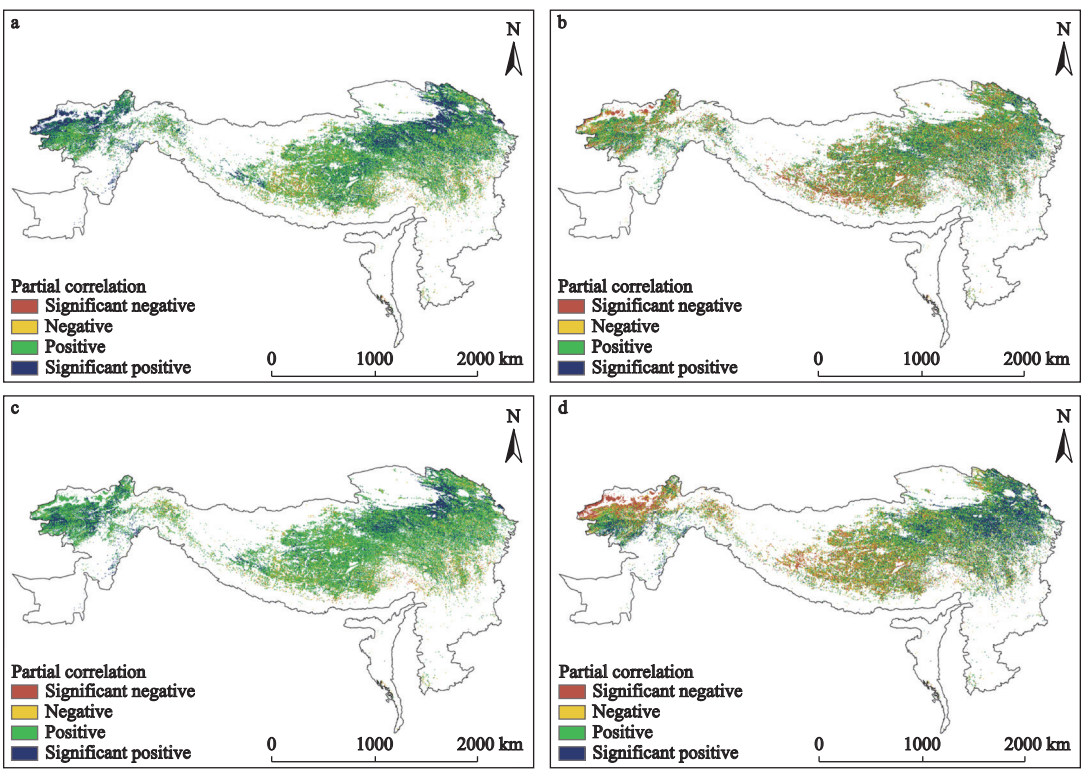

Fig. 8 Partial correlation between grassland AGB and mean annual precipitation (a), annual mean temperature (b), mean precipitation in the growing season (c) and mean temperature in the growing season (d) at the significance level of 0.05 from 2000 to 2018

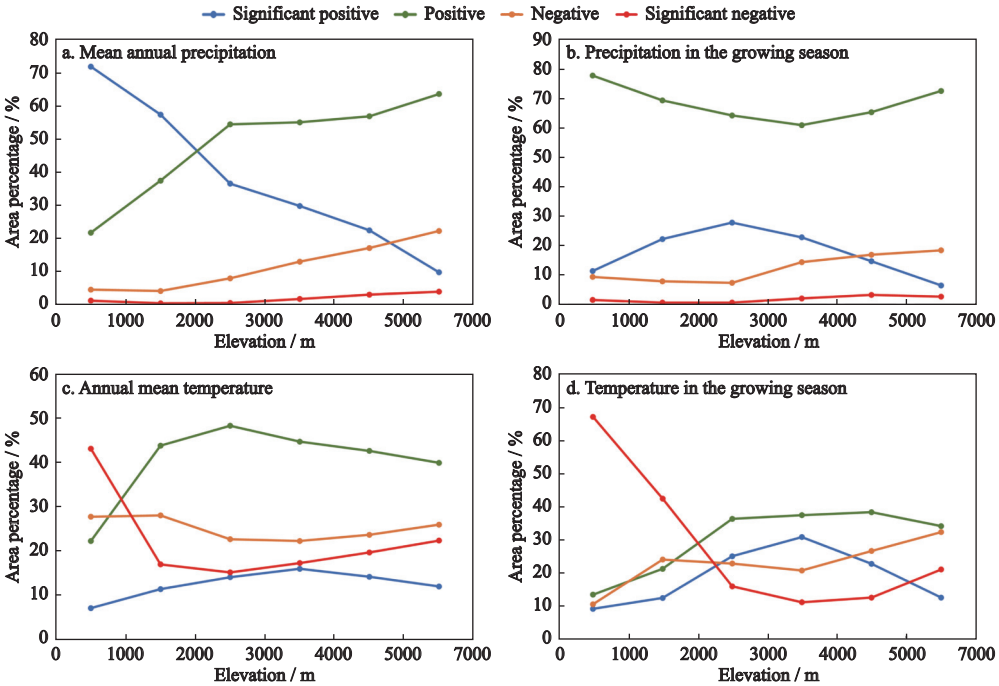

Fig. 9 Area percentage of partial correlation between grassland AGB and climate factors at different elevation ranges

value in the range of 3000–4000 m (Fig. 9c). However, the area percentage of grassland where AGB was significantly negatively correlated with mean annual temperature showed the opposite trend, and the area percentage was highest when the elevation was below 1000 m (43.1%). For the growing season, there were similar parabolic trends for the change in the area percentage of grassland where AGB was significantly positively correlated with precipitation or temperature. In contrast, the largest proportion of grassland area with a significant negative correlation between AGB and temperature in the growing season was found at elevations below 1000 m (Fig. 9d). Additionally, the grassland area where precipitation was significantly negatively correlated with AGB was relatively small in each elevation range for the two temporal scales.

The combined effects of precipitation and temperature fluctuations and their respective contributions to the interannual changes in regional mean grassland AGB from 2000 to 2018 were further quantified by VPA (Fig. 10). By comparing the spatial distribution of the combined effects of climate change on the annual and growing season scales, a similar spatial distribution was found. The grassland AGB was strongly influenced by the climate in the northern part of the Qinghai-Tibet Plateau and the western part of the HKH region, with an $R^2 > 0.5$, and precipitation contributed more than 40% to the climate in these two regions. By comparison, the grassland in the central region (including northern Tibet and the northern foothills of the Himalayas) showed a lower correlation with the comprehensive influence of climate at the two temporal scales. Our results showed that the temperature in the growing season contributed more than that at the annual scale, contributing more than 40% on the eastern Qinghai-Tibet Plateau, while its contribution was mostly concentrated in the range of 10%–30% at the annual scale. Additionally, the grassland area where precipitation contributed more, which accounted for 64.6% of the total grassland area, far exceeded the temperature-dominated area, which accounted for 35.0% of the total grassland area, at the annual scale. A similar performance was also obtained in the growing season (60.3% and 39.3%, respectively).

In terms of the variation in grassland area, the contributions of each climatic factor to grassland AGB changes differed greatly at elevations below 2000 m at the two temporal scales, but their contributions tended to be consistent at elevations above 2000 m (Fig. 11). In the whole HKH region, the grassland area percentage where temperature contributed more than precipitation showed an obvious increasing tendency with elevation at the annual scale, while a trend of an inverted parabola occurred in the growing season. The changes in the grassland area with a greater contribution of precipita-

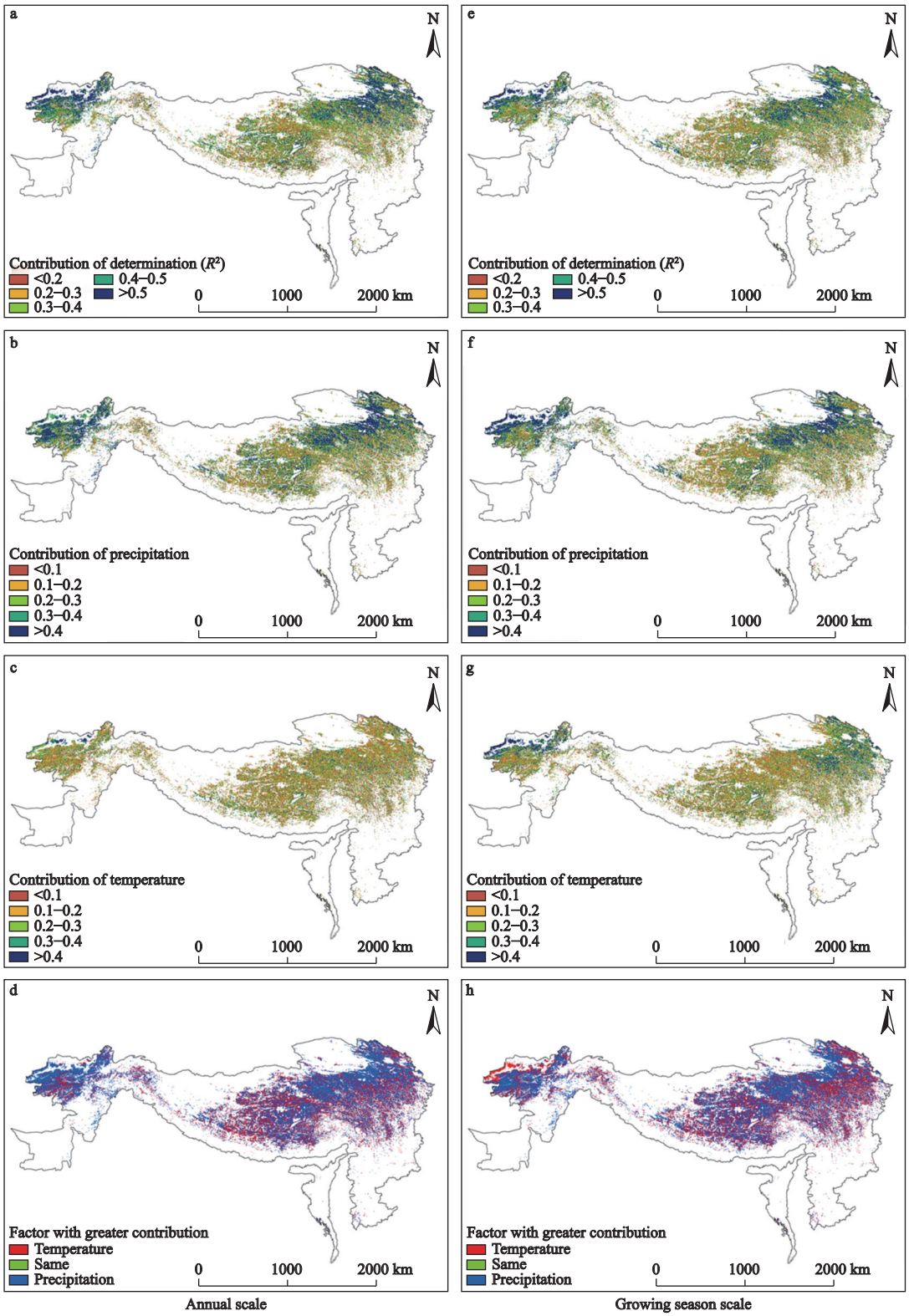

Fig. 10 Spatial distribution of the contribution of climate factors to the interannual change of grassland aboveground biomass (AGB) at two temporal scales. The coefficient of determination between AGB and two climate factors (a, e), the contribution of precipitation (b, f), the contribution of temperature (c, g) and the climate factors with greater contributions (d, h)

tion reversed the trend of temperature at the two temporal scales. Moreover, the grassland area proportion with a greater contribution of precipitation than of temperature to AGB change was higher at each elevation range ex-

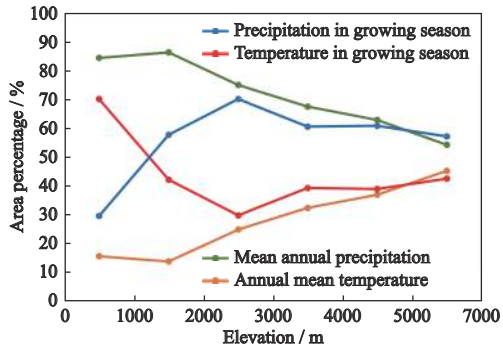

Fig. 11 Area percentage of climate factors with greater contributions at different elevations

cept below 1000 m.

4 Discussion

4.1 Estimation uncertainties of AGB by remote sensing

Accurate estimation of grassland AGB is of great significance for assessing the carbon cycle of grassland ecosystems. Our results demonstrated that the PVIM was feasible for estimating grassland AGB in the HKH region. For example, even though there were no sampling sites in the western region, our grassland AGB results (144.9 g/m^2) were highly consistent with those of a previous study in Pakistan (150 g/m^2), which is located in this region (Ishaq et al., 2019). The difference between the predicted and observed AGB mainly was mainly attributable to two sources. The first source was the fuzzy distribution of grassland types, as the calibration coefficient between the vegetation indices and grassland AGB in the PVIM usually varied between different grassland types because the AGB of different grassland types differed greatly under the same conditions (Li et al., 2016), and there could have been an estimation error using the same coefficient over all the grassland areas. Although the grassland types in some subareas of the HKH region have been classified, such as those on the Qinghai-Tibet Plateau in China (Ren et al., 2008; Wen et al., 2010; Wu et al., 2016), different studies have had inconsistent definitions of the grassland types, and it was also uncertain whether these grassland classification systems were applicable to the entire HKH region. Studies on grassland type classifications should be carried out throughout the HKH region by analyzing the differences between varied grassland types in this region from multiple perspectives, which could improve the estimation accuracy of AGB. Another source of error is the scale effect. The spatial resolution of the MODIS data was 250 m; therefore, the complex topography of the HKH region could have led to a large slope within a pixel, resulting in the underestimation of AGB (Balthazar et al., 2012). At the same time, the inconsistency between the sampling scale and spatial resolution of MODIS could also have caused an estimation error to a certain extent due to location deviation and grassland habitat heterogeneity (Xu et al., 2021), but it might not have been eliminated completely even if the sampling sites were representative enough as each pixel covered a large area. Therefore, satellite data with higher spatial resolutions, such as Landsat and Sentinel-2, coupled with terrain factors could be considered for improving the estimation accuracy of grassland AGB.

4.2 Spatial and temporal variation of grassland AGB

Our results found that there was a decreasing trend of grassland AGB in the HKH region from east to west, and climate factors were considered the main reason for the obvious spatial difference. In terms of the Qinghai-Tibet Plateau, the spatial distribution of grassland AGB was similar to the previous AGB results (Jia et al., 2016) and was consistent with the change in grassland types from alpine meadow to alpine steppe to desert steppe (Wu et al., 2016). Additionally, as the South Asian monsoon is affected by topography, there is more precipitation in the southern Himalayas than in the northwestern Hindu Kush (Panday et al., 2015), which resulted in the opposite performance of grassland AGB in the two subregions.

For the vertical distribution of grassland AGB, some previous studies conducted on the Qinghai-Tibet Plateau or in localized areas of the Central Himalayas showed a negative correlation between grassland AGB and elevation (Jiao et al., 2016; Yadav et al., 2019). However, the correlation was not obvious for the whole region in our study (Fig. 4), which might have been caused by the difference in AGB among subregions. For example, the grassland had both high AGB and high elevation in the southern Himalayas, where the humid climate was beneficial to grassland growth (Hossain and Beierkuhnlein, 2018). In contrast, both grassland AGB and elevation were lower near the Hindu Kush under arid climatic conditions. The complex terrain in the HKH

region causes the climatic conditions of the subregions to be diverse and further influence the vertical distribution of grassland AGB.

During 2000–2018, we found that the mean regional grassland AGB showed a significant increasing trend in the HKH region, which was similar to the results obtained in Qinghai-Tibet Plateau from 2000 to 2011 (Huang et al., 2016) and in the Three-river Headwater Region from 2001 to 2019 (Zhou et al., 2021). Moreover, our results also demonstrated the spatial differences in the trend of grassland AGB between the subregions of the HKH region. Some studies have indicated that variation in climate could lead to changes in grassland AGB or productivity to some extent (Hossain and Beierkuhnlein, 2018; Hossain and Li, 2020) and that climate change is inconsistent in the subregions of the HKH region (Liu et al., 2008), which partly explained the spatial difference in the AGB trends. In addition to climate factors, human-related activities, such as overgrazing, could also cause interannual changes in AGB (Zhang et al., 2017). Moreover, livestock husbandry is the main industry of the HKH region (Shang et al., 2020), which explained why the grassland AGB showed a decreasing trend in several local regions (Fig. 6). By comparison, due to the establishment of the Sanjiangyuan National Natural Reserve in 2000 (Li et al., 2012), the grassland AGB showed a significant increasing trend in the Three-River Headwater Region, and the conservation of the grassland ecosystem resulted in a larger grassland area with a significant increasing trend of AGB in the elevation range of 3000–4000 m to some extent (Fig. 7).

4.3 Influence of precipitation and temperature to grassland AGB variation

Several studies have demonstrated that the effect of climate change on grassland AGB mainly depends on temperature and precipitation (Hu et al., 2011; Wang et al., 2019). According to our results, precipitation mainly had a positive influence on grassland AGB (Fig. 8). Guo et al. (2021b) also demonstrated that grassland productivity had a positive correlation with precipitation in most grasslands of the HKH region. Most of the grassland in the HKH region is in arid and semiarid areas, and it is generally believed that water shortages result in a low leaf area index (LAI) and high root-shoot ratio in these regions, which would severely limit vegetation growth (Bai et al., 2008; Mowll et al., 2015). Therefore, precipitation contributes more than temperature to the variation of the grassland AGB (Fig. 10), which means that precipitation is the main influencing factor for the grassland growth in the HKH region.

In our study, the grassland AGB in response to precipitation and temperature showed spatial heterogeneity and the difference is believed to be related to the climate conditions of the subregions. Zhang et al. (2016) found that precipitation became the main factor influencing productivity in the Three-river Source Region after the 21st century due to a rapid increase in precipitation and Li et al. (2019b) showed that the AGB of the grassland in Tibet was dominated by temperature because of the sustained low precipitation. The differences between the two subregions are consistent with our results. Additionally, the differences in the relative contributions between temperature and precipitation to the change of grassland AGB at different elevation ranges further indicated that different climatic conditions affected the response of the grassland to climate change to some extent (Fig. 11) because the elevation could affect hydrothermal variation (Tao et al., 2015; Munson et al., 2019).

The response of ecosystems to climate change depends on not only the magnitude of the climate but also the timing (Craine et al., 2012; Guo et al., 2021a). Our results indicated that the effects of interannual climate change on grassland AGB were different from those in the growing season. More precipitation in the nongrowing season increased soil moisture and surface runoff partly, and the accumulation of water promoted the growth of the grassland in the growing season (Geruo et al., 2020). The mean annual precipitation showed a more significant positive correlation on grassland than the precipitation in the growing season (Fig. 9). In contrast, the significant promoting effect of temperature change on grassland growth was stronger in the growing season, and Harris (2010) also concluded that the grassland was least affected by temperature in the dormant winter period on the Qinghai-Tibet Plateau. Furthermore, the contribution of temperature change in the growing season to grassland AGB was significantly higher than that of the mean annual temperature at low elevation ranges in the HKH region. Therefore, elevation not only affects the relationships between grassland AGB and climate change but also influences the

contributions of different climate factors to grassland AGB.

4.4 Limitations and future work

In this study, we only focused on the response of the spatial-temporal distribution of grassland AGB to temperature and precipitation. However, some other climate factors are also considered to affect grassland AGB or productivity, such as evapotranspiration (Zarei et al., 2021), wind (Hopkins and Del Prado, 2007) and solar radiation (Zhang et al., 2016). Moreover, human activities are also important factors affecting grassland AGB (Li et al., 2019a; Xiong et al., 2019; Zheng et al., 2019) and some studies explained these influences from several aspects, including grazing intensity (Chen et al., 2014), the population density (Ding et al., 2022) and distance to settlements (Li et al., 2019a), which should be considered in the future to further assess the spatial-temporal variation in grassland AGB in the HKH region.

Additionally, vegetation expansion occurred in the subnival HKH due to global warming (Anderson et al., 2020), while grassland degradation and desertification also occurred in this region (Liu et al., 2017b; An et al., 2021), which reduced the grassland area; however, these factors were ignored in this study. We suggest that grasslands that experience specific changes should be analyzed separately in the future to evaluate the total grassland AGB changes more accurately in the HKH region.

5 Conclusions

Our study assessed the spatial distribution and interannual changes in grassland AGB based on the PVIM and further quantified the AGB response to temperature and precipitation during 2000–2018 in the HKH region. Grassland AGB showed an increasing trend with 1.57 g/(m^2·yr) during the monitoring period. The spatial distribution had a decreasing trend from east to the west throughout the whole region except for the southern Himalayas and it showed highest total AGB in the elevation range between 4000 m and 5000 m. Compared with temperature, precipitation was regarded as the main factor affecting the temporal and spatial variation in grassland AGB in most grassland of the HKH region. We also found that the effect of mean annual precipitation on grassland AGB was greater than that of precipitation in the growing season, while temperature had the opposite result. With the change of elevation, the contribution of precipitation and temperature on grassland AGB at two temporal scales tended to be consistent. This study was instructive for better understanding the temporal and spatial variation in grassland AGB and its response to climate change in the HKH region.

References

Adams J B, Smith M O, Johnson P E, 1986. Spectral mixture modeling: a new analysis of rock and soil types at the Viking Lander 1 Site. *Journal of Geophysical Research: Atmospheres*, 91(B8): 8098–8112. doi: 10.1029/JB091iB08p08098

An R, Zhang C, Sun M Q et al., 2021. Monitoring grassland degradation and restoration using a novel climate use efficiency (NCUE) index in the Tibetan Plateau, China. *Ecological Indicators*, 131: 108208. doi: 10.1016/j.ecolind.2021.108208

Anderson K, Fawcett D, Cugulliere A et al., 2020. Vegetation expansion in the subnival Hindu Kush Himalaya. *Global Change Biology*, 26(3): 1608–1625. doi: 10.1111/gcb.14919

Bai Y F, Wu J G, Xing Q et al., 2008. Primary production and rain use efficiency across a precipitation gradient on the mongolia plateau. *Ecology*, 89(8): 2140–2153. doi: 10.1890/07-0992.1

Balthazar V, Vanacker V, Lambin E F, 2012. Evaluation and parameterization of ATCOR3 topographic correction method for forest cover mapping in mountain areas. *International Journal of Applied Earth Observation and Geoinformation*, 18: 436–450. doi: 10.1016/j.jag.2012.03.010

Carlyle C N, Fraser L H, Turkington R, 2014. Response of grassland biomass production to simulated climate change and clipping along an elevation gradient. *Oecologia*, 174(3): 1065–1073. doi: 10.1007/s00442-013-2833-2

Chen B X, Zhang X Z, Tao J et al., 2014. The impact of climate change and anthropogenic activities on alpine grassland over the Qinghai-Tibet Plateau. *Agricultural and Forest Meteorology*, 189/190: 11–18. doi: 10.1016/j.agrformet.2014.01.002

Chen H, Zhu Q, Peng C H et al., 2013. The impacts of climate change and human activities on biogeochemical cycles on the Qinghai-Tibetan Plateau. *Global Change Biology*, 19(10): 2940–2955. doi: 10.1111/gcb.12277

Craine J M, Nippert J B, Elmore A J et al., 2012. Timing of climate variability and grassland productivity. *Proceedings of the National Academy of Sciences of the United States of America*, 109(9): 3401–3405. doi: 10.1073/pnas.1118438109

Dai L C, Ke X, Guo X W et al., 2019. Responses of biomass allocation across two vegetation types to climate fluctuations in the northern Qinghai-Tibet Plateau. *Ecology and Evolution*, 9(2): 6105–6115. doi: 10.1002/ece3.5194

Dimri A P, Bookhagen B, Stoffel M et al., 2020. *Himalayan*

Weather and Climate and their Impact on the Environment. Cham: Springer. DOI: 10.1007/978-3-030-29684-1.

Ding L, Li Z W, Shen B B et al., 2022. Spatial patterns and driving factors of aboveground and belowground biomass over the eastern Eurasian steppe. *Science of The Total Environment*, 803: 149700. doi: 10.1016/j.scitotenv.2021.149700

Dong S K, Wen L, Zhu L et al., 2010. Implication of coupled natural and human systems in sustainable rangeland ecosystem management in HKH region. *Frontiers of Earth Science in China*, 4: 42–50. doi: 10.1007/s11707-010-0010-z

Duparc A, Redjadj C, Viard-Crétat F et al., 2013. Co-variation between plant above-ground biomass and phenology in subalpine grasslands. *Applied Vegetation Science*, 16(2): 305–316. doi: 10.1111/j.1654-109X.2012.01225.x

Fick S E, Hijmans R J, 2017. WorldClim 2: new 1-km spatial resolution climate surfaces for global land areas. *International Journal of Climatology*, 37(12): 4302–4315. doi: 10.1002/joc.5086

Ge J, Meng B P, Liang T G et al., 2018. Modeling alpine grassland cover based on MODIS data and support vector machine regression in the headwater region of the Huanghe River, China. *Remote Sensing of Environment*, 218: 162–173. doi: 10.1016/j.rse.2018.09.019

Geruo A, Velicogna I, Zhao M et al., 2020. Satellite detection of varying seasonal water supply restrictions on grassland productivity in the Missouri basin, USA. *Remote Sensing of Environment*, 239: 111623. doi: 10.1016/j.rse.2019.111623

Filho M G, Kuplich T M, De Quadros F L F, 2020. Estimating natural grassland biomass by vegetation indices using Sentinel 2 remote sensing data. *International Journal of Remote Sensing*, 41(8): 2861–2876. doi: 10.1080/01431161.2019.1697004

Guo D, Song X, Hu R et al., 2021a. Grassland type-dependent spatiotemporal characteristics of productivity in Inner Mongolia and its response to climate factors. *Science of The Total Environment*, 775: 145644. doi: 10.1016/j.scitotenv.2021.145644

Guo D, Song X, Hu R et al., 2021b. Large-scale analysis of the spatiotemporal changes of Net Ecosystem Production in Hindu Kush Himalayan Region. *Remote Sensing*, 13(6): 1180. doi: 10.3390/rs13061180

Harris R B, 2010. Rangeland degradation on the Qinghai-Tibetan plateau: A review of the evidence of its magnitude and causes. *Journal of Arid Environments*, 74(1): 1–12. doi: 10.1016/j.jaridenv.2009.06.014

Hopkins A, Del Prado A, 2007. Implications of climate change for grassland in Europe: impacts, adaptations and mitigation options: a review. *Grass and Forage Science*, 62(2): 118–126. doi: 10.1111/j.1365-2494.2007.00575.x

Hossain L, Beierkuhnlein C, 2018. Enhanced aboveground biomass by increased precipitation in a central European grassland. *Ecological Processes*, 7(1): 37. doi: 10.1186/s13717-018-0149-1

Hossain L, Li J F, 2020. Effects of long-term climatic variability and harvest frequency on grassland productivity across five ecoregions. *Global Ecology and Conservation*, 23: e01154. doi: 10.1016/j.gecco.2020.e01154

Hu M Q, Mao F, Sun H et al., 2011. Study of normalized difference vegetation index variation and its correlation with climate factors in the three-river-source region. *International Journal of Applied Earth Observation and Geoinformation*, 13(1): 2433. doi: 10.1016/j.jag.2010.06.003

Huang K, Zhang Y J, Zhu J T et al., 2016. The influences of climate change and human activities on vegetation dynamics in theqinghai-tibetplateau.*RemoteSensing*,8(10):876.doi:10.3390/rs8100876

Ishaq S, Ali H, Ahmad B et al., 2019. Dynamics of above ground herbaceous biomass in high altitude rangelands of pakistan. *Journal of Animal and Plant Sciences*, 29(2): 521–530.

Jarvis A, Reuter H I, Nelson A et al. , 2008. Hole-filled SRTM for the globe Version 4, available from the CGIAR-CSI SRTM 90m database. Available at: http://srtm.csi.cgiar.org

Jia W X, Liu M, Yang Y H et al., 2016. Estimation and uncertainty analyses of grassland biomass in Northern China: comparison of multiple remote sensing data sources and modeling approaches. *Ecological Indicators*, 60: 1031–1040. doi: 10.1016/j.ecolind.2015.09.001

Jiao C C, Yu G R, He N P et al., 2016. Spatial pattern of grassland aboveground biomass and its environmental controls in the Eurasian steppe. *Journal of Geographical Sciences*, 27(1): 3–22. doi: 10.1007/s11442-017-1361-0

Jin Y X, Yang X C, Qiu J J et al., 2014. Remote sensing-based biomass estimation and its spatio-temporal variations in temperate grassland, northern China. *Remote Sensing*, 6(2): 1496–1513. doi: 10.3390/rs6021496

Kandel P, Chettri N, Chaudhary S et al., 2021. Ecosystem services research trends in the water tower of Asia: a bibliometric analysis from the Hindu Kush Himalaya. *Ecological Indicators*, 121: 107152. doi: 10.1016/j.ecolind.2020.107152

Karimi S, Nawaz M A, Naseem S et al., 2021. The response of culturally important plants to experimental warming and clipping in Pakistan Himalayas. *PLoS One*, 16(5): e0237893. doi: 10.1371/journal.pone.0237893

Kong B, Yu H, Du R X et al., 2019. Quantitative estimation of biomass of alpine grasslands using hyperspectral remote sensing. *Rangeland Ecology & Management*, 72(2): 336–346. doi: 10.1016/j.rama.2018.10.005

Li C X, de Jong R, Schmid B et al., 2019a. Spatial variation of human influences on grassland biomass on the Qinghai-Tibetan plateau. *Science of The Total Environment*, 665: 678–689. doi: 10.1016/j.scitotenv.2019.01.321

Li F, Zeng Y, Luo J H et al., 2016. Modeling grassland aboveground biomass using a pure vegetation index. *Ecological Indicators*, 62(3): 279–288. doi: 10.1016/j.ecolind.2015.11.005

Li L H, Zhang Y L, Liu L S et al., 2018. Current challenges in distinguishing climatic and anthropogenic contributions to alpine grassland variation on the Tibetan Plateau. *Ecology and Evolution*, 8(11): 5949–5963. doi: 10.1002/ece3.4099

Li L H, Zhang Y L, Wu J S et al., 2019. Increasing sensitivity of alpine grasslands to climate variability along an elevational

gradient on the Qinghai-Tibet Plateau. *Science of The Total Environment*, 678: 21–29. doi: 10.1016/j.scitotenv.2019.04.399

Li X L, Brierley G J, Shi D J et al. 2012. Ecological Protection and Restoration in Sanjiangyuan National Nature Reserve, Qinghai Province, China. *In: Higgitt D (ed).Perspectives on Environmental Management and Technology in Asian River Basins*. New York: Springer Netherlands, 93–120.

Liu S L, Cheng F Y, Dong S K et al., 2017a. Spatiotemporal dynamics of grassland aboveground biomass on the Qinghai-Tibet Plateau based on validated MODIS NDVI. *Scientific Reports*, 7(1): 4182. doi: 10.1038/s41598-017-04038-4

Liu S L, Zhang Y Q, Cheng F Y et al., 2017b. Response of grassland degradation to drought at different time-scales in qinghai province: spatio-temporal characteristics, correlation, and implications. *Remote Sensing*, 9(12): 1329. doi: 10.3390/rs9121329

Liu W, Guo Q H, Wang Y X, 2008. emporal-spatial climate change in the last 35 years in Tibet and its geo-environmental consequences. *Environmental Geology*, 54(8): 1747–1754. doi: 10.1007/s00254-007-0952-y

Morais T G, Teixeira R F M, Figueiredo M et al., 2021. The use of machine learning methods to estimate aboveground biomass of grasslands: a review. *Ecological Indicators*, 130: 108081. doi: 10.1016/j.ecolind.2021.108081

Mowll W, Blumenthal D M, Cherwin K et al., 2015. Climatic controls of aboveground net primary production in semi-arid grasslands along a latitudinal gradient portend low sensitivity to warming. *Oecologia*, 177(4): 959–969. doi: 10.1007/s00442-015-3232-7

Munson S M, Bunting E L, Bradford J B et al., 2019. Plant production responses to precipitation differ along an elevation gradient and are enhanced under extremes. *Ecosystems*, 22 (4): 699–708. doi: 10.1007/s10021-018-0296-3

Panday P K, Ghimire B, 2012. Time-series analysis of NDVI from AVHRR data over the Hindu Kush-Himalayan region for the period 1982-2006. *International Journal of Remote Sensing*, 33(21): 6710–6721. doi: 10.1080/01431161.2012.692836

Panday P K, Thibeault J, Frey K E, 2015. Changing temperature and precipitation extremes in the Hindu Kush-Himalayan region: an analysis of CMIP3 and CMIP5 simulations and projections. *International Journal of Climatology*, 35(10): 3058–3077. doi: 10.1002/joc.4192

Psomas A, Kneubühler M, Huber S et al., 2011. Hyperspectral remote sensing for estimating aboveground biomass and for exploring species richness patterns of grassland habitats. *International Journal of Remote Sensing*, 32(24): 9007–9031. doi: 10.1080/01431161.2010.532172

Quan X W, He B B, Yebra M et al., 2017. A radiative transfer model-based method for the estimation of grassland aboveground biomass. *International Journal of Applied Earth Observation and Geoinformation*, 54: 159–168. doi: 10.1016/j.jag.2016.10.002

Ran Q W, Hao Y B, Xia A Q et al., 2019. Quantitative assessment of the impact of physical and anthropogenic factors on vegetation spatial-temporal variation in northern Tibet. *Remote Sensing*, 11(10): 1183. doi: 10.3390/rs11101183

Ren J Z, Hu Z Z, Zhao J et al., 2008. A grassland classification system and its application in China. *The Rangeland Journal*, 30(2): 199–209. doi: 10.1071/RJ08002

Ren Y Y, Ren G Y, Sun X B et al., 2017. Observed changes in surface air temperature and precipitation in the Hindu Kush Himalayan region over the last 100-plus years. *Advances in Climate Change Research*, 8(2): 148–156. doi: 10.1016/j.accre.2017.08.001

Rodríguez E, Morris C S, Belz J E, 2006. A global assessment of the SRTM performance. *Photogrammetric Engineering & Remote Sensing*, 72 (3): 249–260. doi: 10.14358/PERS.72.3.249

Schickhoff U, Bobrowski M, Böhner J et al., 2015. Do Himalayan treelines respond to recent climate change? An evaluation of sensitivity indicators. *Earth System Dynamics*, 6(1): 245–265. doi: 10.5194/esd-6-245-2015

Shang Z H, Degen A A, Rafiq M K et al. , 2020. *Carbon Management for Promoting Local Livelihood in the Hindu Kush Himalayan (HKH) Region*. Cham: Springer. DOI: 10.1007/978-3-030-20591-1

Shrestha F, Uddin K, Maharjan S B et al., 2016. Application of remote sensing and GIS in environmental monitoring in the Hindu Kush Himalayan region. *AIMS Environmental Science*, 3(4): 646–662. doi: 10.3934/environsci.2016.4.646

Singh S P, Bassignana-Khadka I, Karky B S et al. , 2011. *Climate Change in the Hindu-Kush Himalayas*: *The State of Current knowledge.* Kathmandu: International Centre for Integrated Mountain Development.

Sun J, Cheng G W, Li W P, 2013. Meta-analysis of relationships between environmental factors and aboveground biomass in the alpine grassland on the Tibetan Plateau. *Biogeosciences*, 10(3): 1707–1715. doi: 10.5194/bg-10-1707-2013

Sun X B, Ren G Y, Shrestha A B et al., 2017. Changes in extreme temperature events over the Hindu Kush Himalaya during 1961-2015. *Advances in Climate Change Research*, 8(3): 157–165. doi: 10.1016/j.accre.2017.07.001

Tang R, Zhao Y T, Lin H L, 2021. Spatio-temporal variation characteristics of aboveground biomass in the headwater of the yellow river based on machine learning. *Remote Sensing*, 13(17): 3404. doi: 10.3390/rs13173404

Tao J, Zhang Y J, Dong J W et al., 2015. Elevation-dependent relationships between climate change and grassland vegetation variation across the Qinghai-Xizang Plateau. *International Journal of Climatology*, 35(7): 1638–1647. doi: 10.1002/joc.4082

Todd S W, Hoffer R M, Milchunas D G, 1998. Biomass estimation on grazed and ungrazed rangelands using spectral indices. *International Journal of Remote Sensing*, 19(3): 427–438. doi: 10.1080/014311698216071

Wang L, Yu H Y, Zhang Q et al., 2018. Responses of aboveground biomass of alpine grasslands to climate changes on the Qinghai-Tibet Plateau. *Journal of Geographical Sciences*, 28(12): 1953–1964. doi: 10.1007/s11442-019-1573-y

Wang X M, Dong J J, Baoyin T G T et al., 2019. Estimation and climate factor contribution of aboveground biomass in inner mongolia's typical/desert steppes. *Sustainability*, 11(23): 6559. doi: 10.3390/su11236559

Wei P J, Chen S Y, Wu M H et al., 2021. Increased ecosystem carbon storage between 2001 and 2019 in the northeastern margin of the Qinghai-Tibet Plateau. *Remote Sensing*, 13(19): 3986. doi: 10.3390/rs13193986

Wen Q K, Zhang Z X, Liu S et al., 2010. Classification of grassland types by MODIS time-series images in Tibet, China. *IEEE Journal of Selected Topics in Applied Earth Observations and Remote Sensing*, 3(3): 404–409. doi: 10.1109/Jstars.2010.2049001

Wester P, Mishra A, Mukherji A et al. , 2019. *The Hindu Kush Himalaya Assessment—Mountains, Climate Change, Sustainability and Peopl*e. Cham: Springer. DOI: : 10.1007/978-3-319-92288-1

Wick A F, Geaumont B A, Sedivec K K et al., 2016. Grassland degradation. Biological and environmental hazards, risks, and disasters. *Amsterdam: Elsevier*, 257–276.

Wu B F, Zeng Y, Zhao D, 2016. Land cover mapping and above ground biomass estimation in China. In: *Proceedings of 2016 IEEE International Geoscience and Remote Sensing Symposium*. Beijing, China: IEEE.

Xiong Q L, Xiao Y, Halmy M W A et al., 2019. Monitoring the impact of climate change and human activities on grassland vegetation dynamics in the northeastern Qinghai-Tibet Plateau of China during 2000-2015. *Journal of Arid Land*, 11(5): 637–651. doi: 10.1007/s40333-019-0061-2

Xu D W, Wang C, Chen J et al., 2021. The superiority of the normalized difference phenology index (NDPI) for estimating grassland aboveground fresh biomass. *Remote Sensing of Environment*, 264: 112578. doi: 10.1016/j.rse.2021.112578

Xu J C, Badola R, Chettri N et al. , 2019. *Sustaining Biodiversity and Ecosystem Services in the Hindu Kush Himalaya.* In: Wester P, Mishra A, Mukherji A et al. (eds). *The Hindu Kush Himalaya Assessment.* Cham: Springer, 127−165. DOI: 10.1007/978-3-319-92288-1_5

Xu J C, Grumbine R E, Shrestha A et al., 2009. The melting Himalayas: cascading effects of climate change on water, biodiversity, and livelihoods. *Conservation Biology*, 23(3): 520–530. doi: 10.1111/j.1523-1739.2009.01237.x

Xu X K, Chen H, Levy J K, 2008. Spatiotemporal vegetation cover variations in the Qinghai-Tibet Plateau under global climate change. *Chinese Science Bulletin*, 53(6): 915–922. doi: 10.1007/s11434-008-0115-x

Yadav R P, Gupta B, Bhutia P L et al., 2019. Biomass and carbon budgeting of land use types along elevation gradient in Central Himalayas. *Journal of Cleaner Production*, 211: 1284–1298. doi: 10.1016/j.jclepro.2018.11.278

Yang S X, Feng Q S, Liang T G et al., 2018. Modeling grassland above-ground biomass based on artificial neural network and remote sensing in the Three-River Headwaters Region. *Remote Sensing of Environment*, 204: 448–455. doi: 10.1016/j.rse.2017.10.011

Yang Y K, Xiao P F, Feng X Z et al., 2017. Accuracy assessment of seven global land cover datasets over China. *ISPRS Journal of Photogrammetry and Remote Sensing*, 125: 156-173. doi: 10.1016/j.isprsjprs.2017.01.016

Yao T D, Thompson L G, Mosbrugger V et al., 2012. Third pole environment (TPE). *Environmental Development*, 3: 52–64. doi: 10.1016/j.envdev.2012.04.002

Yu R Y, Yao Y J, Wang Q et al., 2021. Satellite-Derived Estimation of Grassland Aboveground Biomass in the Three-River Headwaters Region of China during 1982–2018. *Remote Sensing*, 13(15): 2993. doi: 10.3390/rs13152993

Zarei A, Chemura A, Gleixner S et al., 2021. Evaluating the grassland NPP dynamics in response to climate change in Tanzania. *Ecological Indicators*, 125: 107600. doi: 10.1016/j.ecolind.2021.107600

Zeng N, Ren X L, He H L et al., 2021. Estimating the grassland aboveground biomass in the Three-River Headwater Region of China using machine learning and Bayesian model averaging. *Environmental Research Letters*, 16(11): 114020. doi: 10.1088/1748-9326/ac2e85

Zhang W J, Zhang F, Qi J G et al., 2017. Modeling impacts of climate change and grazing effects on plant biomass and soil organic carbon in the Qinghai-Tibetan grasslands. *Biogeosciences*, 14(23): 5455–5470. doi: 10.5194/bg-14-5455-2017

Zhang Y, Zhang C B, Wang Z Q et al., 2016. Vegetation dynamics and its driving forces from climate change and human activities in the Three-River Source Region, China from 1982 to 2012. *Science of the Total Environment*, 563–564: 210–220. doi: 10.1016/j.scitotenv.2016.03.223

Zheng K, Wei J Z, Pei J Y et al., 2019. Impacts of climate change and human activities on grassland vegetation variation in the Chinese Loess Plateau. *Science of the Total Environment*, 660: 236–244. doi: 10.1016/j.scitotenv.2019.01.022

Zhou W, Li H R, Xie L J et al., 2021. Remote sensing inversion of grassland aboveground biomass based on high accuracy surface modeling. *Ecological Indicators*, 121: 107215. doi: 10.1016/j.ecolind.2020.107215